Bioconjugate Chemistry

Article

pubs.acs.org/bc

Specific Immobilization of Biotinylated Fusion Proteins NGF and Sema3A Utilizing a Photo-Cross-Linkable Diazirine Compound for Controlling Neurite Extension

Aleesha M. McCormick, Asanka Wijekoon, and Nic D. Leipzig*

Department of Chemical and Biomolecular Engineering, The University of Akron, Akron, Ohio, United States

Supporting Information

ABSTRACT: In this study we report the successful synthesis of *N*-(2-mercaptoethyl)-3-(3-methyl-3*H*-diazirine-3-yl) propanamide (N-MCEP-diazirine), with sulfhydryl and amine photoreactive ends to allow recombinant protein tethering to chitosan films. This regimen allows mimicry of the physiological endeavor of axon pathfinding in the nervous system where neurons rely on cues for guidance during development and regeneration. Our strategy incorporates strong covalent and noncovalent interactions, utilizing N-MCEP-diazirine, maleimide−streptavidin complex, and two custom biotinylated-fusion proteins, nerve growth factor (bNGF), and semaphorin3A (bSema3A). Synthetic yield of N-MCEP-diazirine was 87.3 ± 1.9%. Characteristic absorbance decrease at 348 nm after N-MCEP-diazirine exposure to UV validated the photochemical properties of the diazirine moiety, and the attachment of cross-linker to chitosan films was verified with Fourier transform infrared spectroscopy (FTIR). Fluorescence techniques showed no significant difference in the detection of immobilized proteins compared to absorbing the proteins to films ($p < 0.05$); however, *in vitro* outgrowth of dorsal root ganglia (DRG) was more responsive to immobilized bNGF and bSema3A compared to adsorbed bNGF and bSema3A over a 5 day period. Immobilized bNGF significantly increased DRG length over time ($p < 0.0001$), but adsorbed bNGF did not increase in axon extension from day 1 to day 5 ($p = 0.4476$). Immobilized bSema3A showed a significant decrease in neurite length (524.42 ± 57.31 μm) at day 5 compared to adsorbed bSema3A (969.13 ± 57.31 μm). These results demonstrate the superiority of our immobilization approach to protein adsorption because biotinylated-fusion proteins maintain their active confirmation and their tethering can be spatially controlled via a UV activated N-MCEP-diazirine cross-linker.

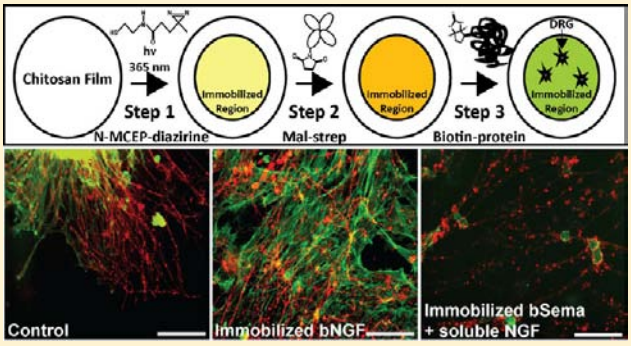

INTRODUCTION

During nervous system development and patterning endogenous proteins play a vital role in guidance and formation of mature neural networks. Additionally, trauma to the nervous system activates many of these endogenous attractive and repulsive biomolecules that overall aim to protect the body and nervous system from further damage. Often, this results in the formation of an environment that is impermissive for axon reinnervation and regeneration. In the peripheral nervous system (PNS), neurons are known to regenerate slowly, about 2 mm/day,[1] whereas central nervous system (CNS) neurons rarely exhibit any regeneration. Neural regeneration strategies for both the PNS and CNS should tailor a microenvironment that mimics physiologic conditions conducive for axon pathfinding to accelerate regeneration (for reviews, see refs 2,3).

The growth cone is unique to neurons and is responsible for properly guiding axons to their target during development and regeneration. The primary cues that steer growth cones are extracellular matrix molecules and attractive and repulsive biomolecules, such as neurotrophins, netrins, ephrins, and semaphorins. These molecules can be tethered to or soluble in this environment, working in conjunction with one another to guide axons in forming a functional nervous system (for review, see ref 4). Nerve growth factor (NGF) was one of the first cytokines/growth factors ever identified since it circulates throughout the body as a vital survival factor (for review, see ref 5). During development, NGF encourages axon outgrowth and guidance, aiding in the development and maintenance of both the PNS and CNS.[6,7] Semaphorin3A (Sema3A) is recognized for its ability to initiate growth cone collapse and is distributed temporally, from development to adulthood, and spatially throughout the nervous system, steering axons along proper nerve tracts and inhibiting them from entering undesired regions.[8,9] Even though Sema3A is considered mainly a chemorepellant protein, its presence in the nervous system is vital in maneuvering and pruning axons during pathfinding, especially for reducing aberrant branching.[10,11]

Received: January 30, 2013
Revised: July 23, 2013
Published: August 5, 2013

   dx.doi.org/10.1021/bc400058n | *Bioconjugate Chem.* 2013, 24, 1515−1526

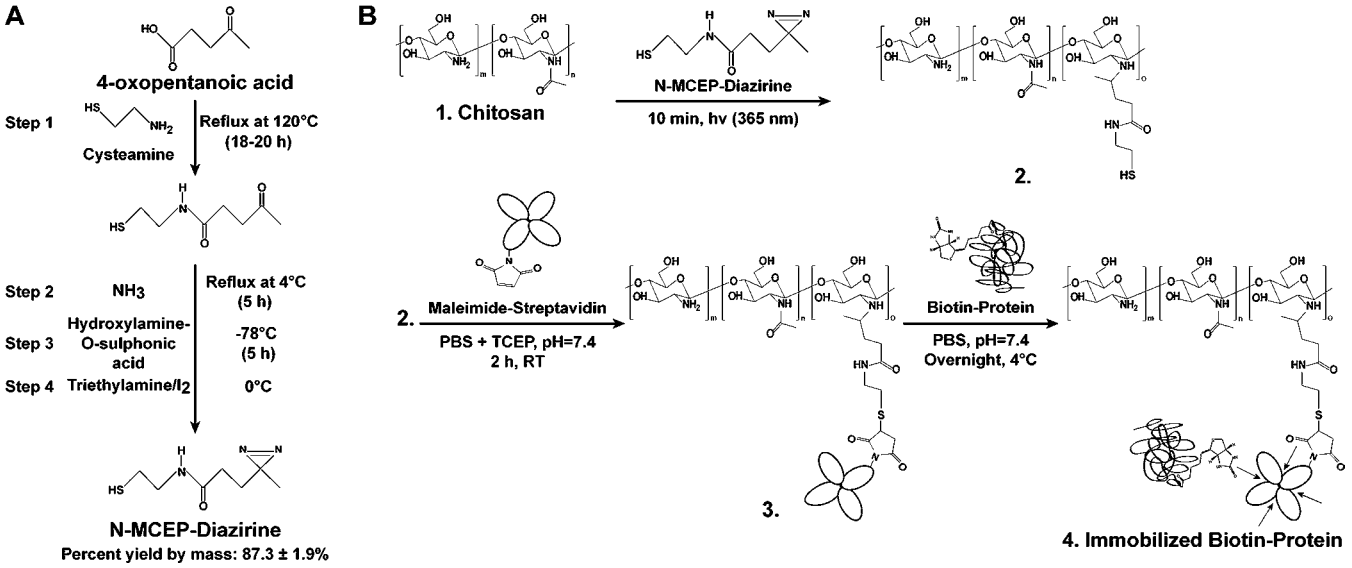

Figure 1. (A) N-MCEP-diazirine synthesis was performed in the dark starting with 4-oxopentanoic acid and involved a series of reactions to produce the desired UV reactive diazirine moiety. (B) Immobilization regime for biotinylated-fusion proteins of NGF and Sema3A. First N-MCEP-diazirine is covalently attached to the primary amines of the chitosan film after exposure to UV light (365 nm). Next the free sulfhydryl end of the cross-linker forms a covalent bond with maleimide. Finally, streptavidin attaches to the biotin located on the N-terminus of either NGF or Sema3A, creating a strong noncovalent interaction that does not dissociate under biological conditions.

Immobilization of biomolecules is important for biosensors, microfluidic devices, and biochemical and biological studies including regenerative treatments. Immobilization provides increased sensitivity and specificity of design, producing high-throughput systems translatable to many bioengineering applications.[12−14] More specifically, protein immobilization has expanded in the past decade through advancements in microcontact and inkjet printing, as well as soft lithography and photolithography techniques, creating tailored micro- and nanofunctionalized surfaces (for review, see ref 15). Functional and stable protein immobilization schemes minimize non-specific protein adsorption while controlling attachment through covalent and bioaffinity interactions.[16,17] These immobilization methods are key for functional presentation of proteins to cell surface receptors and can be utilized to spatially control their active locations. Of specific interest to neural tissue engineering, custom recombinant proteins have been specifically immobilized to induce stem cell differentiation[18,19] and axon guidance.[20,21]

The main objective of this study was to demonstrate that immobilized custom NGF and Sema3A fusion proteins can be created and utilized to control neurite extension and branching. We hypothesized that our immobilization scheme will result in stable, functional fusion proteins, and that immobilized NGF will increase neurite outgrowth and branching, whereas immobilized Sema3A will inhibit axon extension while minimizing branching. In this study, a novel heterobifunctional cross-linker, *N*-(2-mercaptoethyl)-3-(3-methyl-3*H*-diazirine-3-yl) propanamide (N-MCEP-diazirine), was synthesized and implemented to specifically attach custom NGF and Sema3A with UV light to a chitosan substrate, and resulting bioactivity was tested with dorsal root ganglia (DRG).

MATERIALS AND METHODS

Heterobifunctional Cross-Linker Synthesis and Characterization. N-MCEP-diazirine was synthesized (Figure 1A) by mixing 5.80 g 4-oxopentanoic acid (Sigma, St. Louis, MO, USA) and 3.85 g cysteamine (Sigma) in 20 mL ddH_2O and then refluxing overnight at 120 °C. Next the product was purified by flash chromatography to remove unreacted chemicals. The intermediate structure was confirmed with proton (^{1}H) and carbon (^{13}C) NMR and the product was freeze-dried. To add the diazirine moiety we followed similar procedures previously described.[22] Briefly, 1.326 g of the freeze−dried product was refluxed with 100 mL of 3% ammonia solution (J.T. Baker, Phillipsburg, NJ, USA) at 4 °C for 5 h. The temperature of the reaction flask was then reduced to −78 °C and hydroxylamine-*O*-sulfonic acid solution (Sigma) was slowly added (1.6 g to 10 mL) and stirred for 5 h. Then the reaction mixture was stirred at room temperature (RT) overnight to evaporate excess ammonia. The suspension was filtered and washed with 50 mL CH_3OH (Mallinckrodt Baker Inc., Phillipsburg, NJ, USA). The elution was treated with triethylamine (Sigma), cooled to 0 °C, and titrated with I_2 solution (Sigma). The crude product was purified by flash chromatography. The entire synthesis was completed in the dark because exposure to low wavelength light is destructive to certain intermediates and the final product. Test samples for NMR were prepared by weighing 15 mg of sample and dissolving it into 800 μL of $CDCl_3$ (Cambridge Isotope Laboratories Inc., Andover, MA, USA). The structure was confirmed through ^{1}H and ^{13}C NMR (Mercury 300; Varian, Palo Alto, CA, USA).

The photochemical properties of N-MCEP-diazirine were examined over time using a UV spectrophotometer (Infinite M200, Tecan Systems, Grödig, Austria). Samples were prepared in 50:50 volumes of methanol:ultrapure water at 0.5 mg/mL and absorbance was measured with a cuvette at 348 nm with no UV and after exposure to 60, 300, and 600 s of UV with a 3.4 mW/cm^2 UV lamp (365 nm).

AviTag-Sema3A and AviTag-NGF Cloning and Expression. AviTag-NGF (aNGF; 29,322 Da, NCBI accession P25427.2 amino acids 122−241) and AviTag-Sema3A (aSema3A; 91,387 Da, NCBI accession NP_059006 amino

dx.doi.org/10.1021/bc400058n | *Bioconjugate Chem.* 2013, 24, 1515−1526

acids 21−747) fusion proteins were designed by obtaining active sequences from NCBI, incorporating a 6X histadine (His), biotin tag (AviTag), and flexible hinge regions,[19] and were inserted into the isopropyl β-D-1-thiogalactopyranoside (IPTG) inducible pET21a(+) vector integrating ampicillin resistance. Chemically competent *E. coli* BL21 cells (Novagen Inc., Madison, WI, USA) were transformed in accordance to the vendor's instructions with either aNGF plasmid or aSema3A plasmid. Transformed cells were selected on Lysogeny broth (LB; BioShop, Burlington, ON, Canada) agar plates containing 100 μg/mL of ampicillin (Sigma). A single colony of transformed cells was inoculated in LB medium containing 100 μg/mL of ampicillin and was grown up overnight (16 h) in a Thermo Scientific MaxQ 4000 incubated shaker (Thermo Scientific, Rockford, IL, USA) at 300 rpm at 37 °C. The following day, test expressions were performed using 200 μL of the overnight culture to inoculated 5 mL LB medium containing 100 μg/mL ampicillin. Once an optical density at 600 nm (OD_{600}) of 0.8 was reached, cells were induced with 1 mM IPTG (Chem-Impex International, Wood Dale, IL, USA). aSema3A was expressed for 4 h at 37 °C, and aNGF was induced overnight at 18 °C.

Protein sodium dodecyl sulfate polyacrylamide gel electrophoresis (SDS-PAGE) was performed to reveal if proteins were expressed in the soluble or insoluble fractions. For insoluble analysis, Bugbuster (EMD Chemicals Inc., San Diego, CA, USA) was added to the 1000 μL *E. coli* pellet and incubated at RT for 30 min. After centrifugation, 50 μL of supernatant was added to 50 μL Laemmli sample buffer (Bio-Rad, Hercules, CA, USA) containing β-mercaptoethanol (Chem-Impex International). 200 μL of the sample buffer was directly added to the 500 μL pellet for soluble analysis, and all samples were placed in boiling water for 5 min. Then samples were loaded on a Mini-PROTEAN-TGX precast gel (Bio-Rad) using a Mini Format 1-D Electrophoresis System (Bio-Rad). Gels were stained with SimplyBlue SafeStain (Life Technologies, Grand Island, NY, USA), washed, and imaged.

For the main culture, recombinant protein expression followed similar methods as described for the test expression. An overnight grow-up of transformed BL21 *E. coli* cells was used to inoculate 1.8 L of fermentation medium containing 85.7 g terrific broth (BioShop), 28.8 mL 50% glycerol (BioShop), and 100 μg/mL ampicillin and was then cultured at 37 °C with air sparging. After reaching an OD_{600} of 0.8, aSema3A was induced with 1 mM IPTG at 37 °C for 4 h and aNGF was expressed overnight at 18 °C.

Purification and Biotinylation of AviTag-NGF and AviTag-Sema3A. For native (soluble) isolation of aSema3A, the main culture was centrifuged (Beckman Avanti J-26 XPI, JLA 8.1 rotor, 7500 rpm, 4 °C, 15 min, Beckman Coulter, Fullerton, CA, USA) and the resulting *E. coli* pellet was resuspended in lysis buffer (50 mM Tris-HCl (Sigma), 500 mM NaCl (Sigma), 5 mM imidazole (Chem-Impex International), pH = 7.5). *E. coli* were kept on ice and sonicated at 30% output for five pulses of 30 s on and 30 s off. For non-native (insoluble) isolation of aNGF, harvested *E. coli* were centrifuged as described above at RT, resuspended in denaturation buffer (6 M guanidine(Gu)-HCl (Chem-Impex International), 100 mM NaH_2PO_4 (Sigma), 10 mM Tris-HCl, 10 mM imidazole, pH = 8.0) and incubated overnight at RT. The resulting mixtures were then centrifuged (JA 25.5 rotor, 20 000 rpm, 30 min, Beckman Coulter).

The supernatant was then incubated with 2 mL of nickel-nitrilotriacetic acid (Ni-NTA) resin solution (Thermo Scientific) and incubated for at least 1 h, 4 °C for aSema3A and RT for aNGF, and then loaded into a chromatography column. aSema3A was washed ten times with 10 mL wash buffer (50 mM Tris-HCl, 500 mM NaCl, 30 mM imidazole, pH = 7.5) and aNGF was washed similarly with denaturation buffer. aSema3A was eluted 4 times with 5 mL native elution buffer (50 mM Tris-HCl, 500 mM NaCl, 250 mM imidazole, pH = 7.5), whereas aNGF was eluted two times with 15 mL non-native elution buffer (6 M GuHCl, 200 mM acetic acid (EMD Chemicals Inc.)).

aSema3A solution was placed in 50 000 Da MWCO dialysis membranes (SpectraPor, Spectrum Laboratories, Rancho Dominguez, CA, USA) and dialyzed at 4 °C against phosphate buffered saline (PBS, pH = 7.4) containing 2 mM dithiothreitol (DTT; Chem-Impex International) for 4 h and switched to fresh buffer overnight. aNGF was dialyzed at 4 °C against PBS containing 0.2 mM GuHCl and 2 mM DTT (pH = 7.4) using a 25 000 Da MWCO dialysis membrane. After 4 h the membrane containing aNGF was placed in fresh buffer (PBS, pH = 7.4) overnight. Each protein was concentrated to 3−5 mL and further purified using fast protein liquid chromatography (FPLC, ÄKTA purifier with Frac-950 and Superdex 200 prep grade column, GE Healthcare, Piscataway, NJ, USA). Protein concentration was determined with a UV spectrophotometer (Tecan Systems) for aSema3A and aNGF by measuring the absorbance at 280 nm and calculated using a molar extinction coefficient of 99 710 $L{\cdot}mol^{-1}{\cdot}cm^{-1}$ and 47 510 $L{\cdot}mol^{-1}{\cdot}cm^{-1}$, respectively.

aSema3A and aNGF were biotinylated using biotin ligase BirA500 (Avidity, Aurora, CA, USA) following the company's protocol to create bSema3A and bNGF fusion proteins. Biotinylation was quantified using the FluoReporter Biotin Quantification assay kit (Life Technologies). Functionality of biotinylated proteins was determined by binding biotinylated proteins to streptavidin (Thermo Scienctific) and running a Native PAGE. First, streptavidin was incubated with four times the amount of bSema3A and bNGF at RT for 3 h. Native PAGE cathode (0.1 M Tris-base and 0.1 M tricine (both Sigma)) and anode (0.2 M Tris-base, pH = 8.9) running buffers and a 6X sample buffer (175 mM Tris-HCl, 40% glycerol, 0.25% bromophenol blue (Bio-Rad)) were made. Then 2 μL of sample buffer was added to 15 μL of protein samples. Native PAGE was run at 4 °C until the samples were located at the bottom of the electrophoresis gel (Mini-PROTEAN-TGX precast gel). These gels were stained with Coomassie blue for 2 h at RT and destained overnight and the following day before imaging.

Chitosan Film Preparation. Chitosan films were prepared according to ref 23. Briefly, medium molecular weight chitosan (Sigma), with 82% degree deacetylation was dissolved at 2 wt% in 2 v/v% acetic acid/ddH_2O on a shaker overnight. Enough chitosan solution was then transferred into well plates (diameters of 11 mm and 35 mm) in order to cover the bottom of the dish and dried in a fume hood overnight. The films were neutralized for 30 min in ammonium hydroxide solution (NH_4OH:ddH_2O:CH_3OH at 3:7:90), then washed three times in PBS. Films were sterilized in 70% ethanol for 30 min and then rinsed in PBS.

For cell adhesion, laminin (Life Technologies) was covalently bound through the linkage of the carboxylic acid amino acid residues of laminin to the primary amines of

chitosan by reacting 5 μg/mL of the protein with 5 mM 1-ethyl-3-(3-dimethylaminopropyl) carbo-diimide (EDC; Chem-Impex International) and 50 mM *N*-hydroxysulfosuccinimide (sulfo-NHS; Chem-Impex International) for 1 h at RT. Films were rinsed in PBS before cell culture.

Immobilization of Biotin-NGF and Biotin-Sema3A on Chitosan Films. Our targeted and specific immobilization of biotin-proteins to chitosan films is depicted in Figure 1B. First, chitosan films were prepared in well-plates, dried, neutralized, and washed as described above. Then, 25 mM of N-MCEP-diazirine was added to the films and placed under a UV lamp (365 nm) for 10 min. Films were washed with PBS containing 50 mM DTT three times for at least 30 min each wash and were then rinsed in PBS three times to remove DTT. Maleimide-streptavidin (mal-strep; 0.200 μM, Sigma) was applied and incubated on the films for 2 h at RT and then washed in PBS + 20 mM Tris (2-carboxyethyl) phosphine hydrochloride (TCEP; Chem-Impex International) three more times for at least 30 min each wash. bNGF and bSema3A were applied to films overnight at 4 °C to achieve protein tethering. This process is referred to as immobilized groups throughout the text.

Fourier transform infrared spectroscopy (FTIR) was performed for confirmation of our immobilization process of biotinylated protein to chitosan films using a Nicolet-6700 (Thermo Scientific) with 10 co-added scans at resolution of 4 cm^{-1}. Chitosan films were prepared in a 48-well plate (d = 11 mm), freeze−dried overnight, and separate films were scanned at RT. Immobilized and adsorbed samples were generated for each group with chitosan films serving as the control. The immobilized samples represented each stage in the attachment process described above: (i) chitosan film + N-MCEP-diazirine, (ii) chitosan film + N-MCEP-diazirine + mal-strep, and (iii) chitosan film + N-MCEP-diazirine + mal-strep + biotin-protein. Biotin-proteins were added to films at a concentration of 10 μg/mL. The three adsorbed groups paralleled this attachment process; however, the N-MCEP-diazirine was not exposed to UV light in any of the samples but kept in the dark for the incubation period of 10 min. An additional group of biotin-protein was adsorbed to chitosan films as well and represents how either adsorbed bNGF or adsorbed bSema3A was presented in DRG extension studies described below.

Quantification of Immobilized Biotin-NGF and Biotin-Sema3A. For quantification of immobilization both bNGF and bSema3A were fluorescently labeled with 5(6)-carboxyfluorescein, succinimidyl ester (5(6)-FAM SE; Biotium, Hayward, CA, USA). Fifty times molar excess of 5(6)-FAM SE was added to either bNGF or bSema3A and reacted for 3 h at 4 °C. The reaction solution was dialyzed (10 000 Da MWCO) against PBS (pH = 7.4) and switched to fresh buffer 6 times over a 2 d period. Chitosan films were prepared in a 48-well plate, and four groups (with n = 4) were set up for fluorescent quantification of 5(6)-FAM SE biotin-proteins: (i) immobilized N-MCEP-diazirine + mal-strep + biotin-protein, (ii) adsorbed N-MCEP-diazirine + mal-strep + biotin-protein, (iii) adsorbed mal-strep + biotin-protein, and (iv) adsorbed biotin-protein. The immobilized group (i) was the only group where N-MCEP-diazirine was exposed to UV. For group (ii), N-MCEP-diazirine was incubated for 10 min in the dark before washing. For groups (iii) and (iv), mal-strep was applied to films for 2 h at RT and washed in PBS. 5(6)-FAM SE bNGF and bSema3A were added to films at 1, 3, and 10 μg/mL. After protein incubation overnight, films were washed rigorously with Tris buffered saline with Tween 20 (TBST; 20 mM Tris-HCl, 150 mM NaCl, 0.1% Tween 20, pH = 7.5) injected through a 16G needle 15 times and left in buffer on a shaker for 1 h. Vigorous washing with TBST was repeated two more times. Chitosan films were finally rinsed in PBS three times. Films were freeze-dried overnight and samples were weighed out for each group and dissolved in 2 v/v% acetic acid/ddH_2O overnight. Fluorescent intensity measurements (Ex/Em: 495/525) were measured using a fluorescent microplate reader and protein concentrations were determined via comparison to standard curves made from fluorescently tagged proteins.

For spatial patterning and further fluorescent quantification, chitosan films were dried in 6-well plates (d = 35 mm), neutralized, and washed as described above. Silicone isolators (JTR13R-2.0-Press-To-Seal Silicone Isolator, Grace Bio-Laboratories, Bend, OR, USA) were placed inside 6-well plates to make a circular pattern. 5(6)-Carboxy-X-rhodamine-C5-maleimide (5(6)-ROX-C5-maleimide; Biotium) was used to examine attachment of N-MCEP-diazirine. Four groups were used to analyze this immobilization process: (i) immobilized N-MCEP-diazirine +5(6)-ROX-C5-maleimide, (ii) immobilized N-MCEP-diazirine + mal-strep +5(6)-FAM SE biotin-protein, (iii) adsorbed N-MCEP-diazirine +5(6)-ROX-C5-maleimide, and (iv) adsorbed N-MCEP-diazirine + mal-strep +5(6)-FAM SE biotin-protein. N-MCEP-diazirine was exposed to UV for 10 min for immobilized groups and kept in the dark for the same amount of time for adsorbed groups. 5(6)-ROX-C5-maleimide was added at 10 μM in PBS + 20 mM TCEP (pH = 7.4) for 2 h at RT. Films were washed extensively as described above with TBST. Silicone isolators were removed and films were imaged using a fluorescent microscope (Olympus IX81, Tokyo, Japan) and attachment was quantified using average intensity values over the imaged area.

Dorsal Root Ganglia Dissection and Culture on Immobilized Protein Surfaces. The following twelve groups were created for cell experimentation with varied attachment methods and proteins as described above: (i) control, (ii) control + soluble mouse NGF (Sol mNGF), (iii) control + Sol bSema3A, (iv) control + Sol mNGF + Sol bSema3A, (v) adsorbed (Ad) bNGF, (vi) immobilized (Im) bNGF, (vii) Ad bSema3A, (viii) Im bSema3A, (ix) Ad bNGF + Sol mNGF, (x) Im bNGF + Sol mNGF, (xi) Ad bSema3A + Sol mNGF, and (xii) Im bSema3A + Sol mNGF. For immobilized groups, bSema3A and bNGF were applied to films to achieve saturation concentrations of 91.39 ng/mL[24] and 100 ng/mL.[23]

DRG were isolated from chicken embryos (postfertilization day 9) and harvested in Hanks Balanced Salt Solution (HBSS, Life Technologies). Whole DRG were cleaned of any debris and placed into well plates containing serum free medium (13.4 g/L DMEM (Dulbecco's Modified Eagles Medium), 1.176 g/L sodium bicarbonate, 1% L-glutamine (Life Technologies), 1% streptomycin−penicillin (Life Technologies), 5 μg/mL human insulin, 5 μg/mL transferrin, 3×10^{-8} M sodium selenite, 100 μM putrescine, 2×10^{-8} M progesterone, all Sigma). After 4 h, 6-well plates were carefully flooded with media containing mitotic inhibitors to reach a final volume of 2 mL per well and a final concentration of 4 μM for both mitotic inhibitors, uridine (Chem-Impex International), and 5-Fluoro-2-deoxyuridine (Chem-Impex International). Select groups also contained 10 ng/mL soluble mNGF and 91.39 ng/mL of soluble bSema3A.[24] Bright-field microscope images (Olympus) were obtained at day 1 and 5.

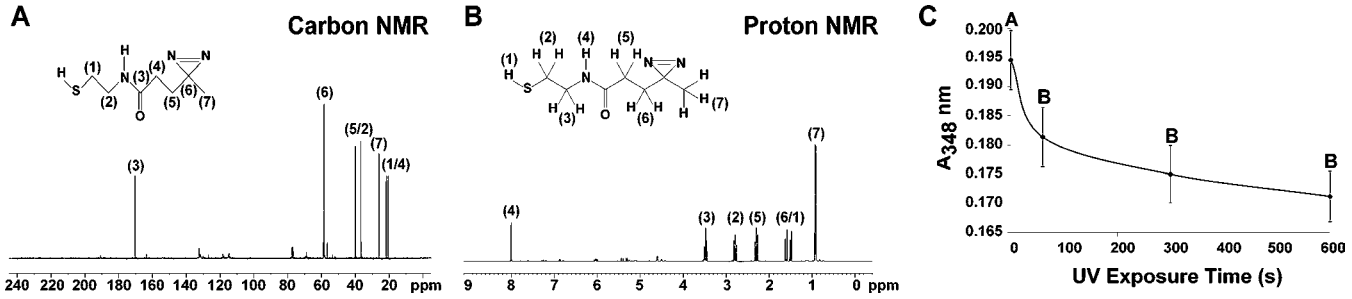

Figure 2. High resolution ^{13}C NMR (A) and ^{1}H NMR (B) spectra of N-MCEP-diazirine dissolved in $CDCl_3$ confirm high purity of the synthesized heterobifunctional cross-linker. (C) Absorbance at 348 nm of N-MCEP-diazirine in 50:50 methanol:ultrapure water decreases significantly (p = 0.0018) after UV exposure (365 nm) for 60, 300, and 600 s as a result of degradation of the diazirine moiety.

At day 5, DRG were fixed in 3.7% paraformaldehyde for 5 h and rinsed in PBS. Permeabilization was achieved with 0.1% Triton X-100 (Sigma) in PBS added for 5 min, and then samples were rinsed with PBS. Blocking buffer of 10% FBS (Life Technologies) in PBS was used at RT for 1 h. Samples were rinsed with PBS and incubated with the primary antibody, monoclonal mouse anti-β-III tubulin (1:1000, Covance, Princeton, NJ, USA), for 1 h. Next DRG were washed in PBS for 15 min and incubated with secondary goat anti-mouse IgG AlexaFluor 546 (1:400, Life Technologies) for 1 h and washed in PBS for another 15 min. AlexaFluor 488 phallodin (1:200, Life Technologies) was added for 2 h at RT and washed in PBS for 15 min. Finally, cell nuclei were stained with 10 μM Hoechst 33342 (Life Technologies) for 10 min and PBS was kept on the samples for imaging with a fluorescent microscope (Olympus IX81).

Statistical Analysis. For N-MCEP-diazirine characterization and immobilization quantification, a single factor analysis of variance (ANOVA) was performed with JMP Pro 9.0 software. This data is reported as mean ± standard deviation (SD). Significance was established with an α level of 0.05.

Further statistical analysis for neurite length and number calculations was performed with SAS 9.2 software where a three-way factor ANOVA was used to analyze the effect of factor interaction of the following: type of protein, attachment method, and time. Seven combinations of factors are examined: (i) protein, (ii) attachment, (iii) day, (iv) protein*attachment, (v) protein*day, (vi) attachment*day, and (vii) protein*attachment*day. If these interactions were revealed to be significant (F-value < 0.05) then they were further analyzed using the Tukey-Kramer method. The type of protein contained six levels: (i) control, (ii) bNGF, (iii) bSema3A, (iv) mNGF (only used in soluble form), (v) bNGF/mNGF, and (vi) bSema3A/mNGF. Attachment method also contained six levels: (i) none, (ii) Ad, (iii) Im, (iv) Sol (mNGF and bSema3A were used in soluble form), (v) Ad/Sol, and (vi) Im/Sol. Two time points (day 1 and 5) were included in analyses. The p-values between these groups were analyzed in a pairwise comparison and an α level of 0.05 was used. Data for neurite length and number is given by least-squares mean (lsmean) ± standard error (SE).

RESULTS

NMR and Absorbance Characterization of N-MCEP-Diazirine. High resolution ^{1}H and ^{13}C NMR spectra were obtained to confirm the structure of the resulting product, N-MCEP-diazirine (Figure 2A,B). These spectra show no additional peaks confirming structure of the target compound and indicating high purity. Additionally, N-MCEP-diazirine absorbance at 348 nm before UV irradiation (0.195 ± 0.005 nm) significantly decreased after 60, 300, and 600 s of UV (365 nm), 0.181 ± 0.005 nm, 0.175 ± 0.005 nm, and 0.171 ± 0.004 nm, respectively (Figure 2C).

Purification and Biotinylation of AviTag-NGF and AviTag-Sema3A. The designed fusion proteins aNGF and aSema3A integrate an N-terminal 6X His tag for isolation using Ni-NTA affinity chromatography. The elution product from affinity chromatography was concentrated and further purified by FPLC allowing a single aNGF fraction (Figure 3A) and

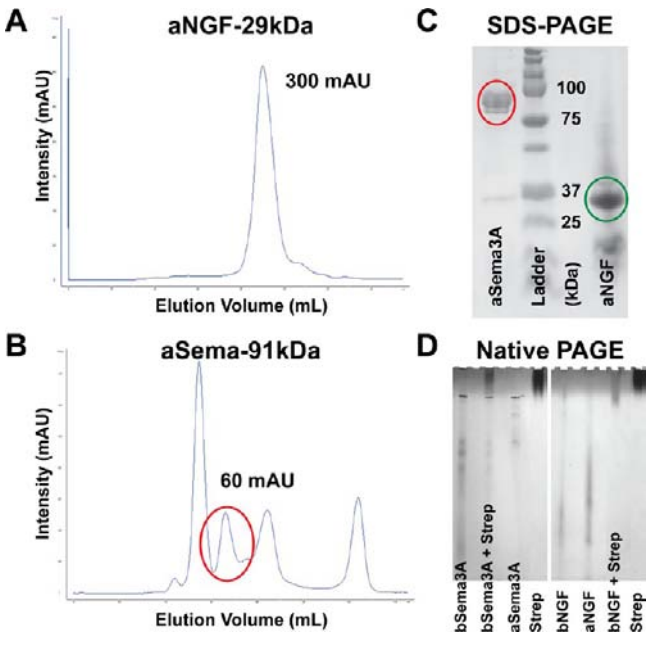

Figure 3. Isolation and purification of aNGF and aSema3A. The FPLC peaks were collected for aNGF (A) and aSema3A (B, indicated by circle) buffered in PBS (pH = 7.4). (C) The elutions from these peaks were concentrated to approximately 1 mg/mL and a sample (40 μL) was mixed with 20 μL Laemmli buffer containing β-mercaptoethanol and boiled for 5 min. SDS-PAGE shows aSema3A (red circle) and aNGF (green circle) after FPLC purification. (D) Native PAGE shows the conjugation of bSema3A and bNGF to streptavidin (Strep). Four times the amount of bSema3A and bNFG (based on molarity) was added to streptavidin. Streptavidin controls were added to the wells at 10 times the molarity of the bSem3A + Strep and bNGF + Strep conjugates. bSema3A is double the concentration of bSema3A + Strep and aSema3A. All the NGF lanes contain similar concentrations. At least 0.5 μg protein/band was loaded into each lane.

dx.doi.org/10.1021/bc400058n | Bioconjugate Chem. 2013, 24, 1515−1526

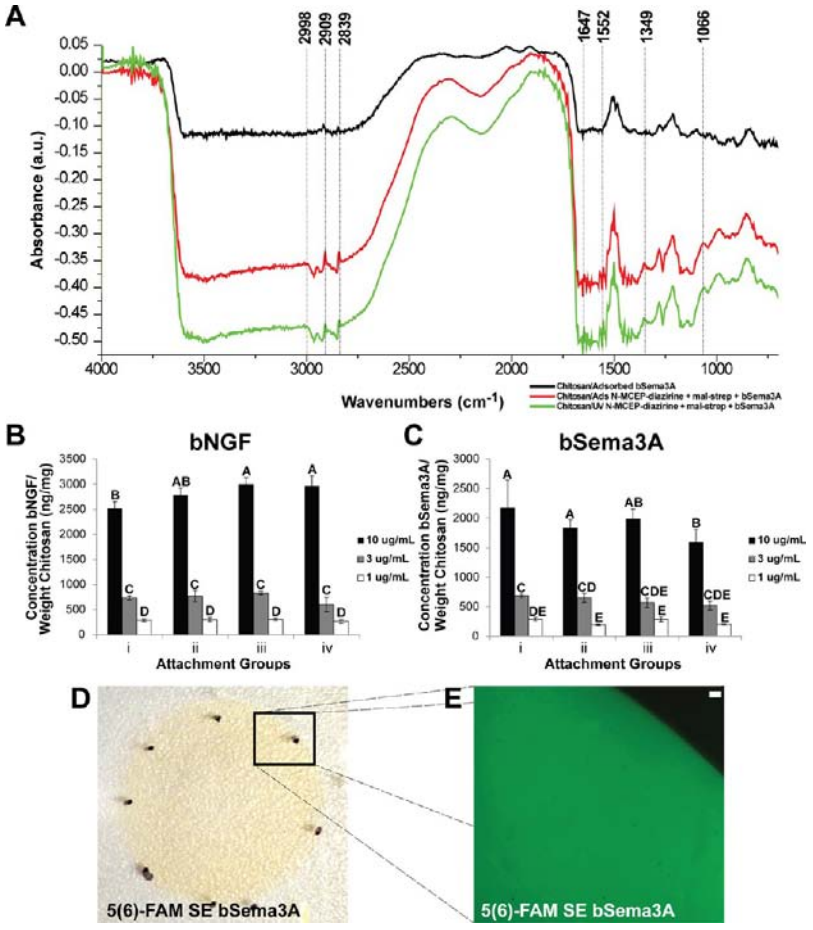

Figure 4. Immobilization quantification and spatial patterning of biotinylated proteins. (A) Absorbance spectra of surface functional groups for bSema3A attachment in respect to the chitosan control film; where Abs = $\log(I_{\text{chitosan film}}/I_{\text{attachment group}})$. bSema3A was either adsorbed to the chitosan films or added to the films after N-MCEP-diazirine adsorption or irradiation and mal-strep addition. The two attachment groups' spectra show CH and amide bond bending and stretching, which is not apparent in the adsorbed bSema3A spectrum. (B–C) After immobilization, films were weighed and dissolved in 2 V/V% acetic acid and run against a standard curve of fluorescently labeled biotin-protein. Immobilization quantification of 5(6)-FAM SE tagged bNGF and bSema3A show significant differences (denoted by letters) between the immobilized concentrations, but these differences vary between attachment groups at the same concentration. The above groups are: (i) immobilized N-MCEP-diazirine + mal-strep + biotin-protein, (ii) adsorbed N-MCEP-diazirine + mal-strep + biotin-protein, (iii) adsorbed mal-strep + biotin-protein, and (iv) adsorbed biotin-protein. (D) Picture of patterned immobilized 5(6)-FAM SE bSema3A at a concentration of 0.20 mg/mL using a silicone isolator. (E) Fluorescent image of portion of 5(6)-FAM SE bSema3A at 4×. Scale bar = 100 μm.

aSema3A fraction (Figure 3B) to be collected and confirmed through SDS-PAGE (Figure 3C). Biotinylation of 100% for each protein was achieved and confirmed with the FluoReporter Biotin Quantification assay kit. The functionality of these biotinylated proteins was confirmed with Native PAGE (Figure 3D) after bSema3A and bNGF were conjugated to streptavidin. Conjugation was performed by incubating the proteins together for 3 h in PBS (pH 7.4). The bSema3A-streptavidin lane shows some bSema3A not conjugated with the streptavidin, but there is no bNGF detected in the bNGF-streptavidin lane. Streptavidin, aSema3aA, aNGF, bSema3A, and bNGF were run next to these lanes as a reference.

Quantification of Biotin-NGF and Biotin-Sema3A Immobilization to Chitosan Films. bNGF and bSema3A were immobilized to chitosan films using N-MCEP-diazirine heterobifunctional cross-linker (Figure 1B). FTIR was used to verify the attachment for each step of the immobilization process for bSema3A and bNGF (Figure 4A, S1). The absorbance spectrum of each addition was generated using chitosan film as the control reference. There is no noticeable difference between the spectra of immobilized bSema3A (N-MCEP diazirine exposed to UV + mal-strep + bSema3A) compared to the adsorbed three step attachment of N-MCEP diazirine + mal-strep + bSema3A (Figure 4A). However, these spectra are different from those generated from just adsorbing bSema3A to the chitosan surfaces (Figure 4A). An increase in asymmetrical and symmetrical CH stretching is seen in the wavenumber region 2840–3000 cm^{-1} and CH deformation at 1349 cm^{-1} for the immobilized and adsorbed attachment groups, but it is not as prominent when only bSema3A is adsorbed to the chitosan film. Also, a CO absorption peak is seen at 1066 cm^{-1} for the two attachment groups but not for adsorbed bSema3A. The wavenumber region from 1510 to 1700 cm^{-1} exhibits characteristic bending and stretching of amide I and II bonds as shown by adsorption peaks in the attachment groups at 1647 cm^{-1} and 1552 cm^{-1}, respectively. Similar spectra are seen with bNGF attachment as well (Figure S1).

After adding labeled bNGF and bSema3A at 1, 3, and 10 μg/mL to chitosan films, protein attachment was confirmed using a spectrophotometer for immobilized group (i) and adsorbed groups (ii-iv). For bNGF, there was a significant difference

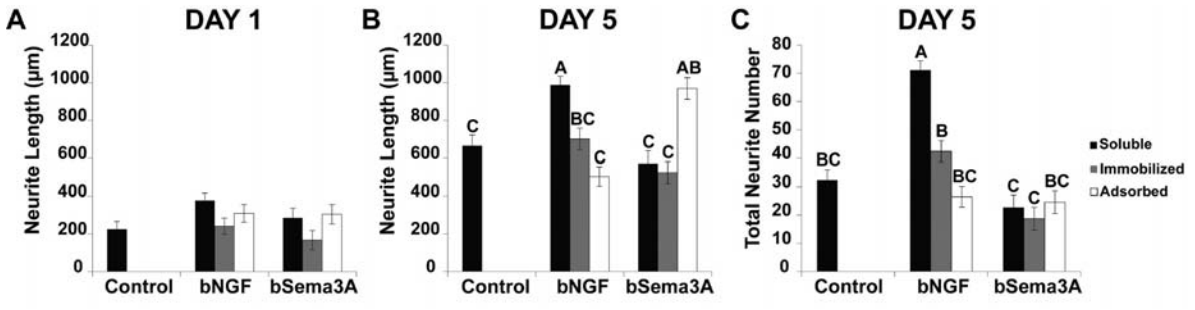

Figure 5. Results of neurite length and number between soluble (black), immobilized (gray), and adsorbed (white) biotinylated proteins. Accompanying statistical analysis is presented in the Supporting Information. (A-B) Lengths of neurites for days 1 and 5, respectively. Overall neurite length increased from day 1 to 5 except for Sol bSema3A and Ad bNGF. Day 1 resulted in no significant differences between groups. At day 5, Im bSema3A and Sol bSema3A caused a significant decrease in length compared to Ad bSema3A groups. (C) Total neurite number for each group at day 5. Sol mNGF resulted in the most neurites, and Im bNGF had significantly more neurites than Im bSema3A and Sol bSema3A. Values shown in figure are given by lsmean ± SE, and significance between groups is denoted by letters. Each group contained a sample size of 3 to 9 DRG.

between each concentration of protein added (Figure 4B). At 10 μg/mL significantly less bNGF was detected for group (i) compared to groups (iii) and (iv). There were some significant differences between concentrations for bSema3A (Figure 4C). However, at 10 μg/mL group (i) had significantly more bSema3A attachment compared to groups (iii) and (iv). Attachment of spatially patterned 5(6)-ROX-C5-maleimide and 5(6)-FAM SE bSema3A (Figure 4C-D) was quantified using average fluorescent intensity values from a fluorescent microscope. Immobilized 5(6)-ROX-C5-maleimide has significantly more attachment ($p < 0.05$) compared to adsorbed 5(6)-ROX-C5-maleimide; however, immobilized 5(6)-FAM SE bSema3A is not different from adsorbed 5(6)-FAM SE bSema3A (Figure S2).

Neurite Number and Length Analysis of Dorsal Root Ganglion on Immobilized Protein. Neurite number and length of DRG were analyzed in *ImageJ* software for day 1 and 5 of *in vitro* culture. The most important significance values regarding neurite length and number will be compared and discussed (Figure 5); however, comparison and statistical outcomes for all the groups are provided in the Supporting Information.

For neurite length analysis, protein*attachment*day was a significant combination ($p < 0.0021$), and a pairwise comparison was analyzed for this combination, since all three factors together affected length, making individual factor analysis inappropriate (Results S3). Length data for days 1 and 5 (Figure 5A-B) shows a significant difference in time for all the groups except Ad bNGF ($p = 0.4476$) and Sol bSema3A ($p = 0.1149$). There is no significance in lengths between groups at day 1 (Figure 5A). However, at day 5 more significant differences are seen, as Sol mNGF (987.29 ± 46.80 μm) is significantly different from all groups (Figure 5B) except for Ad bSema3A (969.13 ± 57.31 μm). Also at day 5, Ad bSema3A (969.13 ± 57.31 μm) has significantly longer neurites than the control (665.08 ± 57.31 μm), Ad bNGF (504.15 ± 51.26 μm), Sol bSema3A (572.97 ± 66.18 μm), and Im bSema3A (524.42 ± 57.31 μm).

Neurite number analysis showed a significance for time ($p < 0.0177$) as well as protein*attachment ($p < 0.0001$). A Student's t test showed no significance in neurite number between days 1 and 5 ($p = 0.3195$). The Tukey-Kramer method was used to analyze significance between protein*attachment interaction (Results S4), and total neurite number measurements are given in Figure 5C. Sol mNGF has significantly more neurites ($p < 0.0001$) compared to other groups. Im bNGF (42.39 ± 3.74) had significantly more neurites compared to both Im bSema3A (18.75 ± 4.01) and Sol bSema3A (22.73 ± 4.36), but interestingly is not significant compared to Ad bSema3A (24.53 ± 4.01). Ad bSema3A/Sol mNGF showed significantly more neurites (77.05 ± 2.90) when compared to Im bSema3A/Sol mNGF (56.73 ± 3.32) and Sol bSema3A/Sol mNGF (62.48 ± 3.23) (Results S4).

Tethered Biotin-Sema3A affects Cytoskeletal Structure of Neurites. At day 5, DRG were fixed, stained, and imaged (Figure 6). Negative controls (Figure 6A,G) provided no bNGF, Sol mNGF, or bSema3A supplement show weak tubulin structure as well as a poor actin cytoskeleton in the extending neurites. DRG provided Sol mNGF (Figure 6B,H) and Im bNGF (Figure 6C,I) show intact microtubules and filamentous actin (F-actin) with intertwined fibers and complex branching. Ad bSema3A (Figure 6D) and Ad bSema3A/Sol mNGF (Figure 6J) maintain some F-actin structure. However, even in the presence of Sol mNGF, Sol bSema3A (Figure 6E,K) and Im bSema3A (Figure 6F,L) illustrate a disrupted cytoskeleton structure with punctate βIII-tubulin and poor F-actin staining resulting in decreased branching and neurite extension.

DISCUSSION

A primary goal of this study was to synthesize N-MCEP-diazirine, a heterobifunctional cross-linking reagent able to link an amine containing substrate to a sulfhydryl/maleimide containing protein or biomolecule. Additionally, we required a linker activated by UV light on one end for the purpose of spatially controlling location and presentation of the conjugated protein or biomolecule for future regenerative guidance applications (Figure 1). Upon activation with UV light (365 nm), N_2 is eliminated and the resulting carbene end of the linker is attached to free amines of chitosan.[25] The addition of soluble mal-strep followed by our biotinylated proteins completed our immobilization scheme allowing us to test neurite activity in response to either soluble or immobilized bNGF and bSema3A. This design is quick, reproducible, and applicable to other materials containing amines or free sulfhydryls and provides a tethering mechanism that does not interfere with the binding of the protein to its corresponding cell-surface receptor.

Application and synthesis of diazirines has greatly impacted the areas of photoaffinity labeling, topography probes,

dx.doi.org/10.1021/bc400058n | *Bioconjugate Chem.* 2013, 24, 1515−1526

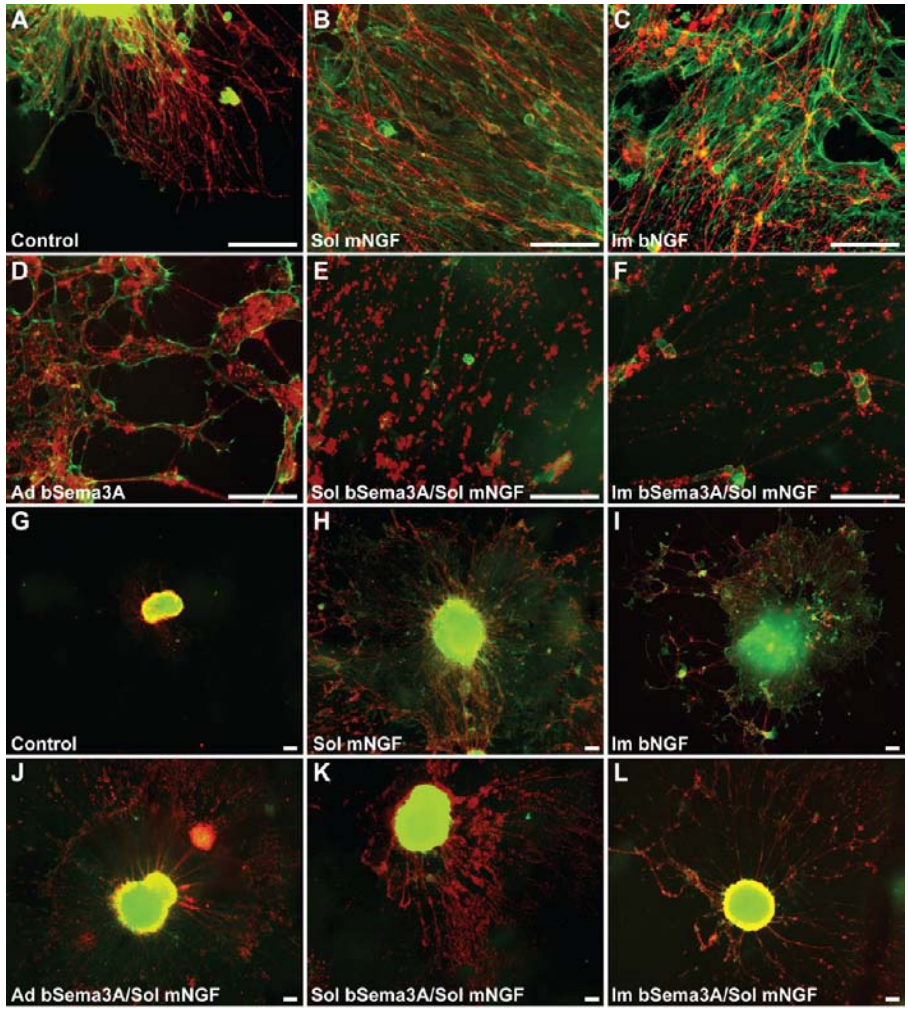

Figure 6. IHC images at day 5 showing bNGF and bSema3A effects on cytoskeletal structure. (A-F) 20× images and (G-L) 4× images. (A,G) Control group with only defined media showing axon cytoskeleton. (B,H) Sol mNGF causes increased branching of neurites and Im bNGF (C,I) shows a similar response. (D) Ad bSema3A and (J) Ad bSema3A/Sol mNGF, respectively, maintain F-actin but (E,K) Sol bSema3A/Sol mNGF and (F,L) Im bSema3A/Sol mNGF show interrupted microtubules and F-actin cytoskeleton. Red = βIII-tubulin and green = F-actin. Scale bar = 100 μm.

bioengineering surfaces, and cross-linking (for reviews see refs 26,27). The decrease in absorbance at 348 nm after UV exposure is characteristic of other diazirine derivatives as a result of the rearrangement of the diazirine into a diazo isomer.[28−30] Diazirines have been incorporated into many macromolecular systems, because upon UV irradiation or ultrasonication, highly reactive carbene residues form stable covalent bonds at room temperature in both acidic and alkaline conditions.[26,30] In previous work, galactose and lactose were immobilized to a polystyrene surface through the photoactivation of a diazirine derivative to examine both hepatocyte and lectin, a sugar binding protein, adhesion to these oligosaccharides.[31] One important finding from this study reveals that cell or protein interaction was affected by not only the type of oligosaccharide, but also the structure and length of spacer of the diazirine derivative.[31] Building on this research, our cross-linker was designed to be bifunctional, providing the proper spacer length for immobilized bNGF and bSema3A to retain their native structure over their adsorbed counterparts. This initial study has afforded us the opportunity to show that specific protein immobilization (Figure 1) is necessary for proper cellular responses. However, the value of UV irradiation in our immobilization process may not be as obvious. We were able to spatially control the location of our immobilized biotin-protein utilizing masking (Figure 4C-D). Photoactivation is beneficial over other patterning techniques because of the length scales and precision it can provide spatially in both two and three dimensions. Adams *et al.* photoimmobilized a peptide forming 10 μm width lines and 30 μm × 100 μm rectangles, which were able to precisely guide and turn DRG.[21] Three-dimensional cell studies utilized two-photon laser microscopy in order to form micropatterns in hydrogels for cell guidance and migration.[32−34] Future studies will aim to achieve similar patterning with our biomaterial-protein systems in order to precisely guide and control axon extension. However, the best approach to patterning and immobilizing peptides/biomolecules could utilize a combination of lithography techniques exploiting UV light, chemical conjugations, and masking (for reviews, see refs 15,35).

Biotinylation of our proteins was detected, and biotin functionality was confirmed with Native PAGE (Figure 3D). bSema3A and bNGF were added in excess to account for the tetrameric streptavidin protein. The light bSema3A band located in the bSema3A-streptavidin lane could be a result of adding too much protein or bSema3A not being 100% biotinylated; however, the majority is biotinylated and

sequestered by streptavidin upon comparison to bSema3A and aSema3A lanes. The potential immunogenicity of streptavidin could be a limitation to translating this strategy *in vivo*. Streptavidin has caused some immune activation when used in clinical pretargeted radioimmunotherapy trials, where biotin derivatives were targeted to tumor sites.[36−38] However, most of these studies have been short-term and the long-term immune response to streptavidin is still unknown. In our experiments low concentrations of streptavidin were used to immobilize biotin-proteins, and there are modifications, such as PEGylation and site-directed mutagenesis, that could be utilized to decrease immunogenic responses to streptavidin.[39−41] Furthermore, biotin-streptavidin represents only one possible conjugation mechanism and was selected as a proof of concept for these studies. Other protein pairs such as human serum albumin−albumin binding domain,[42] barnase−barstar,[34] and even azide−alkyne (click chemistry)[43,44] could be used in a similar manner with our methodology (Figure 1) to supply less immunogenic conjugation mechanisms.

The specific attachment of N-MCEP-diazirine + mal-strep + biotinylated proteins through immobilization and nonspecific adsorption was confirmed with FTIR (Figure 4A, S1). Chitosan films were taken as the background; therefore, absorbance peaks are a result of the changes occurring to the films. The CH stretching and deformation wavenumbers are due to the attachment process and agrees with the literature.[45,46] The appearance of amide bond stretching (1552 cm^{-1} and 1647 cm^{-1}) has been confirmed by others[45−48] and is a result of this linkage present in N-MCEP-diazirine because is it not seen in the adsorbed protein group. However, we did not observe any major changes in absorbance between irradiating and adsorbing N-MCEP-diazirine prior to the addition of mal-strep and biotinylated proteins.

One reason for this similarity could be due to the reactivity of the diazirine moiety. Even though samples were kept in the dark, during the washing stages ambient light could have caused some diazirine activation and/or degradation. We performed experiments on a commercially available diazirine cross-linker (sulfosuccinimidyl 2-([4,4′-azipentanamido]ethyl)-1,3′-dithiopropionate; Thermo Scientific) and observed that at least 10 min were required for its diazirine structure to significantly degrade as measured by a decrease in absorbance at 348 nm (data not shown). Our linker only took 60 s at the same molarity to significantly degrade (Figure 2C). This again shows the sensitivity of our compound to long UV wavelengths. Additionally the similarity between our treatment groups could result from the net positive charge on chitosan strongly attracting each component (N-MCEP-diazirine, mal-strep, and biotinylated protein) and is further discussed below. Most importantly, the findings from FTIR show there is a difference between solely adsorbing and immobilizing a biotinylated protein to the surface of chitosan. As a result, the proteins were presented in these two different forms for the *in vitro* DRG extension study and outgrowth responded differently to each treatment (Figure 5).

We found that our immobilization approach (Figure 1B) resulted in similar bulk protein attachment to the chitosan films compared to adsorbing the protein to the surface (Figure 4B−C, Figure S2). This high concentration of protein adsorption to the chitosan films even after extensive washing, we believe, is due to strong interaction of protein with the positively charged chitosan film. It is important to note that we do not see this protein adsorption behavior in a similar streptavidin−biotinylated-protein tethering system we have developed for a photo-cross-linkable chitosan hydrogel, since both the total material and the number of free amines are significantly reduced.[19] As proteins adsorb to surfaces they can lose their native structure, decreasing their bioactivity.[49] Therefore, in our experiments even though there was no consistent difference between our adsorbed groups and immobilized groups, this does not mean that the adsorbed bNGF and bSema3A are fully bioactive. Furthermore, our data suggest that Ad bNGF and Ad bSema3A decrease or lose bioactivity as they strongly interact with the chitosan surface (Figure 6). This resulted in an increase in neurite length and number for Ad bSema3A, and additionally Ad bNGF did not significantly change its length from day 1 to day 5 where Im bNGF did result in increased neurite extension over time (Figure 5). In any bioengineering strategy it is important for proteins to maintain their conformation for proper protein−protein interaction to activate desired cell signaling pathways.[50−52]

Delivery of soluble growth factors to cell surface receptors (i.e., endocrine, autocrine paracrine signaling, etc.) occurs throughout the body and is vital for tissue maintenance and regeneration (for reviews see refs 53,54). Sema3A, NGF, and other neurotrophins have been extensively studied in their soluble form and are known to affect CNS and PNS neurite outgrowth.[24,55,56] Historically, scientists have utilized soluble growth factors for studying neurite outgrowth *in vitro* since they were originally discovered in soluble form either in the blood or secreted from cells in culture. A major disadvantage of soluble growth factors is shortened biological activity because of either inactivation before reaching their target or down-regulation due to internalization and decomposition inside the cell. More recent research has revealed that tissues and cells can bind to immobilized growth factors to modify their activity, and researchers have begun replicating this in tissue regeneration strategies (for reviews see refs 57,58). Signaling by immobile extracellular matrix molecules as well as membrane-bound proteins, including ephrins and some semaphorins, is extremely important *in vivo*, and unlike soluble factors, they cannot be internalized but are still able to initiate similar signaling pathways through surface bound receptors.[4,59]

Immobilized growth factors can activate intended cellular receptors as may also occur in the body, and can do so for a much longer period of time since they are not degraded by internal cell mechanisms; however, this sustained signaling may activate different pathways than the soluble form since additional signaling can occur when the activated growth factor−receptor complex is internalized and processed.[57,58] As a result, one cannot necessarily expect that an immobilized factor will have identical cellular responses to known soluble responses. Such is the case with responses we observed in this study regarding immobilized NGF. Im bNGF did not produce longer neurite extensions compared to other groups (Figure 5A-B); however, robust axons and intricate branching were seen (Figure 6). The mechanism for terminal branching is not well understood, but results from local NGF activation of PI3K/Akt cascade, initiating actin involved in collateral branching.[60] Our results are similar to other studies where soluble and immobilized NGF favored axon branching over elongation.[61−63] We observed that even though branching was prevalent, neurites elongated over time in the presence of Im bNGF increasing in length from day 1 to 5. This occurrence can be explained by local activation of PI3K[64] and Rac1 and Cdc42[65] producing mostly local outgrowth through reorganiza-

tion and regulation of the actin cytoskeleton. Furthermore, previous work has shown that both NGF inhibition and immobilization still result in local axon outgrowth as well as retrograde survival signals without internalization of NGF.[20,66,67] Given this information, it is likely that Im bNGF in this study activated both branching and elongation pathways; however, we plan to study this in the near future with our methodologies.

To date, few studies have immobilized chemorepellant proteins and examined resulting cellular responses, making the analysis of soluble, immobilized, and adsorbed bSema3A unique to our study. Im bSema3A produced comparable results to how Sol bSema3A acts on neurons in terms of neurite length and number (Figure 5) as well as cytoskeletal changes (Figure 6). IHC images show substantial loss of F-actin and corresponding decreases in total number of neurites and branching in the presence of both Sol bSema3A and Im bSema3A. However, Ad bSema3A retains actin organization, likely because of reduced bioactivity as described above. Our results are consistent with the ability of Sema3A to interrupt actin structures via up-regulation of the actin depolymerase cofilin.[68,69] Our results also agree with a recent study where decreases in phallodin staining in DRG growth cones exposed to soluble Sema3A were observed and shown to directly result from breakdown of F-actin meshwork and partial depolymerization of F-actin bundles.[70]

CONCLUSIONS

Overall our immobilization approach proved to maintain bioactivity of bNGF and bSem3A allowing for growth cone interaction by either locally activating or inhibiting pathway effectors involved in cytoskeletal organization. The immobilization of both proteins using our methodology provided superior neurite growth responses over adsorbing the proteins to our culture surfaces. Herein, we document synthesis of the heterobifunctional cross-linker, N-MCEP-diazirine, which served as a vital molecule for our immobilization strategy, imparting the ability to form stable bonds to the chitosan film substrates through photoactivation. Immobilizing bNGF and bSema3A afforded the ability to manipulate neurite outgrowth and extension by mimicking potential *in vivo* circumstances of receptor−ligand presentation. This method is translatable to other proteins, biomaterials, and cell and tissue types and in the future can be applied to patterning multiple biomolecules in two and three dimensions.

ASSOCIATED CONTENT

Supporting Information

Data pertaining to FTIR attachment of bNGF to chitosan films and the quantification of immobilized 5(6)-ROX-C5-maleimide and 5(6)-FAM SE bSema3A as compared to adsorption to chitosan films. Additionally, graphs and statistical tables are provided showing the trends and significance between all twelve groups regarding neurite length and number analysis. This material is available free of charge via the Internet at http://pubs.acs.org.

AUTHOR INFORMATION

Corresponding Author

*E-mail: nl21@uakron.edu. Telephone: 330-972-6881. Fax: 330-972-5856.

Notes

The authors declare no competing financial interest.

ACKNOWLEDGMENTS

We are grateful for funding from the University of Akron that supported this work. We would like to thank Dr. Rebecca Willits for training in DRG harvest and culture, as well as Elizabeth Endrizzi for all of her help in recombinant protein expression, isolation, and purification. We would also like to acknowledge Dr. Steven Chuang and his students Mathew Isenberg and Seyed Ali Modjtahedi for assistance with FTIR equipment and analysis of spectra.

REFERENCES

(1) Buchthal, F., and Kuhl, V. (1979) Nerve conduction, tactile sensibility, and the electromyogram after suture or compression of peripheral nerve: a longitudinal study in man. *J. Neurol. Neurosurg. Psychiatry 42*, 436−451.

(2) Raivich, G., and Makwana, M. (2007) The making of successful axonal regeneration: genes, molecules and signal transduction pathways. *Brain Res. Rev. 53*, 287−311.

(3) Tohda, C., and Kuboyama, T. (2011) Current and future therapeutic strategies for functional repair of spinal cord injury. *Pharmacol. Ther. 132*, 57−71.

(4) McCormick, A. M., and Leipzig, N. D. (2012) Neural regenerative strategies incorporating biomolecular axon guidance signals. *Annals Biomedical Engineering 40*, 578−597.

(5) Levi-Montalcini, R. (1987) The nerve growth factor: thirty-five years later. *Biosci. Rep. 7*, 681−699.

(6) Heumann, R., Korsching, S., Bandtlow, C., and Thoenen, H. (1987) Changes of nerve growth factor synthesis in nonneuronal cells in response to sciatic nerve transection. *J. Cell Biol. 104*, 1623−1631.

(7) Whittemore, S. R., Ebendal, T., Larkfors, L., Olson, L., Seiger, A., Stromberg, I., and Persson, H. (1986) Development and regional expression of beta nerve growth factor messenger RNA and protein in the rat central nervous system. *Proc. Natl. Acad. Sci. U. S. A. 83*, 817−821.

(8) Luo, Y., Raible, D., and Raper, J. A. (1993) Collapsin: a protein in brain that induces the collapse and paralysis of neuronal growth cones. *Cell 75*, 217−227.

(9) Giger, R. J., Wolfer, D. P., De Wit, G. M., and Verhaagen, J. (1996) Anatomy of rat semaphorin III/collapsin-1 mRNA expression and relationship to developing nerve tracts during neuroembryogenesis. *J. Comp. Neurol. 375*, 378−392.

(10) Tang, X. Q., Heron, P., Mashburn, C., and Smith, G. M. (2007) Targeting sensory axon regeneration in adult spinal cord. *J. Neurosci. 27*, 6068−6078.

(11) Bagri, A., Cheng, H. J., Yaron, A., Pleasure, S. J., and Tessier-Lavigne, M. (2003) Stereotyped pruning of long hippocampal axon branches triggered by retraction inducers of the semaphorin family. *Cell 113*, 285−299.

(12) Wang, J., Onoshima, D., Aki, M., Okamoto, Y., Kaji, N., Tokeshi, M., and Baba, Y. (2011) Label-free detection of DNA-binding proteins based on microfluidic solid-state molecular beacon sensor. *Anal. Chem. 83*, 3528−3532.

(13) Sorribas, H., Padeste, C., and Tiefenauer, L. (2002) Photolithographic generation of protein micropatterns for neuron culture applications. *Biomaterials 23*, 893−900.

(14) Shi, P., Nedelec, S., Wichterle, H., and Kam, L. C. (2010) Combined microfluidics/protein patterning platform for pharmacological interrogation of axon pathfinding. *Lab Chip 10*, 1005−1010.

(15) Ganesan, R., Kratz, K., and Lendlein, A. (2010) Multicomponent protein patterning of material surfaces. *J. Mater. Chem. 20*, 7322−7331.

(16) Jonkheijm, P., Weinrich, D., Kohn, M., Engelkamp, H., Christianen, P. C., Kuhlmann, J., Maan, J. C., Nusse, D., Schroeder, H., Wacker, R., Breinbauer, R., Niemeyer, C. M., and Waldmann, H.

(2008) Photochemical surface patterning by the thiol-ene reaction. *Angew. Chem., Int. Ed. Engl. 47*, 4421−4424.
(17) Vaisocherova, H., Zhang, Z., Yang, W., Cao, Z., Cheng, G., Taylor, A. D., Piliarik, M., Homola, J., and Jiang, S. (2009) Functionalizable surface platform with reduced nonspecific protein adsorption from full blood plasma–material selection and protein immobilization optimization. *Biosens. Bioelectron. 24*, 1924−1930.
(18) Aizawa, Y., Leipzig, N., Zahir, T., and Shoichet, M. (2008) The effect of immobilized platelet derived growth factor AA on neural stem/progenitor cell differentiation on cell-adhesive hydrogels. *Biomaterials 29*, 4676−4683.
(19) Leipzig, N. D., Wylie, R. G., Kim, H., and Shoichet, M. S. (2011) Differentiation of neural stem cells in three-dimensional growth factor-immobilized chitosan hydrogel scaffolds. *Biomaterials 32*, 57−64.
(20) Yu, L. M., Miller, F. D., and Shoichet, M. S. (2010) The use of immobilized neurotrophins to support neuron survival and guide nerve fiber growth in compartmentalized chambers. *Biomaterials 31*, 6987−6999.
(21) Adams, D. N., Kao, E. Y., Hypolite, C. L., Distefano, M. D., Hu, W. S., and Letourneau, P. C. (2005) Growth cones turn and migrate up an immobilized gradient of the laminin IKVAV peptide. *J. Neurobiol. 62*, 134−147.
(22) Van der Meijden, B., and Robinson, J. A. (2011) Synthesis and application of photoproline-a photoactivatable derivative of proline. *ARKIVOC vi*, 130−136.
(23) Yu, L. M., Wosnick, J. H., and Shoichet, M. S. (2008) Miniaturized system of neurotrophin patterning for guided regeneration. *J. Neurosci. Methods 171*, 253−263.
(24) Ben-Zvi, A., Yagil, Z., Hagalili, Y., Klein, H., Lerman, O., and Behar, O. (2006) Semaphorin 3A and neurotrophins: a balance between apoptosis and survival signaling in embryonic DRG neurons. *J. Neurochem. 96*, 585−597.
(25) Gomes, A. F., and Gozzo, F. C. (2010) Chemical cross-linking with a diazirine photoactivatable cross-linker investigated by MALDI- and ESI-MS/MS. *J. Mass Spectrom. 45*, 892−899.
(26) Dubinsky, L., Krom, B. P., and Meijler, M. M. (2012) Diazirine based photoaffinity labeling. *Bioorg. Med. Chem. 20*, 554−570.
(27) Blencowe, A., and Hayes, W. (2005) Development and application of diazirines in biological and synthetic macromolecular systems. *Soft Matter 1*, 178−205.
(28) Weber, T., and Brunner, J. (1995) 2-(Tributylstannyl)-4-[3-(trifluoromethyl)-3H-diazirin-3-yl]benzyl alcohol: a building block for photolabeling and cross-linking reagent of very high specific radioactivity. *J. Am. Chem. Soc. 117*, 3084−3095.
(29) Chee, G. L., Yalowich, J. C., Bodner, A., Wu, X., and Hasinoff, B. B. (2010) A diazirine-based photoaffinity etoposide probe for labeling topoisomerase II. *Bioorg. Med. Chem. 18*, 830−838.
(30) Brunner, J., Senn, H., and Richards, F. M. (1980) 3-Trifluoromethyl-3-phenyldiazirine. A new carbene generating group for photolabeling reagents. *J. Biol. Chem. 255*, 3313−3318.
(31) Chevolot, Y., Martins, J., Milosevic, N., Leonard, D., Zeng, S., Malissard, M., Berger, E. G., Maier, P., Mathieu, H. J., Crout, D. H., and Sigrist, H. (2001) Immobilisation on polystyrene of diazirine derivatives of mono- and disaccharides: biological activities of modified surfaces. *Bioorg. Med. Chem. 9*, 2943−2953.
(32) Luo, Y., and Shoichet, M. S. (2004) A photolabile hydrogel for guided three-dimensional cell growth and migration. *Nat. Mater. 3*, 249−253.
(33) Lee, S. H., Moon, J. J., and West, J. L. (2008) Three-dimensional micropatterning of bioactive hydrogels via two-photon laser scanning photolithography for guided 3D cell migration. *Biomaterials 29*, 2962−2968.
(34) Wylie, R. G., Ahsan, S., Aizawa, Y., Maxwell, K. L., Morshead, C. M., and Shoichet, M. S. (2011) Spatially controlled simultaneous patterning of multiple growth factors in three-dimensional hydrogels. *Nat. Mater. 10*, 799−806.
(35) Rusmini, F., Zhong, Z., and Feijen, J. (2007) Protein immobilization strategies for protein biochips. *Biomacromolecules 8*, 1775−1789.
(36) Weiden, P. L., Breitz, H. B., Press, O., Appelbaum, J. W., Bryan, J. K., Gaffigan, S., Stone, D., Axworthy, D., Fisher, D., and Reno, J. (2000) Pretargeted radioimmunotherapy (PRIT) for treatment of non-Hodgkin's lymphoma (NHL): initial phase I/II study results. *Cancer Biother. Radiopharm. 15*, 15−29.
(37) Knox, S. J., Goris, M. L., Tempero, M., Weiden, P. L., Gentner, L., Breitz, H., Adams, G. P., Axworthy, D., Gaffigan, S., Bryan, K., Fisher, D. R., Colcher, D., Horak, I. D., and Weiner, L. M. (2000) Phase II trial of yttrium-90-DOTA-biotin pretargeted by NR-LU-10 antibody/streptavidin in patients with metastatic colon cancer. *Clin. Cancer Res. 6*, 406−414.
(38) Forero, A., Weiden, P. L., Vose, J. M., Knox, S. J., LoBuglio, A. F., Hankins, J., Goris, M. L., Picozzi, V. J., Axworthy, D. B., Breitz, H. B., Sims, R. B., Ghalie, R. G., Shen, S., and Meredith, R. F. (2004) Phase 1 trial of a novel anti-CD20 fusion protein in pretargeted radioimmunotherapy for B-cell non-Hodgkin lymphoma. *Blood 104*, 227−236.
(39) Chinol, M., Casalini, P., Maggiolo, M., Canevari, S., Omodeo, E. S., Caliceti, P., Veronese, F. M., Cremonesi, M., Chiolerio, F., Nardone, E., Siccardi, A. G., and Paganelli, G. (1998) Biochemical modifications of avidin improve pharmacokinetics and biodistribution, and reduce immunogenicity. *Br. J. Cancer 78*, 189−197.
(40) Marshall, D., Pedley, R. B., Boden, J. A., Boden, R., Melton, R. G., and Begent, R. H. (1996) Polyethylene glycol modification of a galactosylated streptavidin clearing agent: effects on immunogenicity and clearance of a biotinylated anti-tumour antibody. *Br. J. Cancer 73*, 565−572.
(41) Meyer, D. L., Schultz, J., Lin, Y., Henry, A., Sanderson, J., Jackson, J. M., Goshorn, S., Rees, A. R., and Graves, S. S. (2001) Reduced antibody response to streptavidin through site-directed mutagenesis. *Protein Sci. 10*, 491−503.
(42) Wylie, R. G., and Shoichet, M. S. (2011) Three-dimensional spatial patterning of proteins in hydrogels. *Biomacromolecules 12*, 3789−3796.
(43) Khatwani, S. L., Kang, J. S., Mullen, D. G., Hast, M. A., Beese, L. S., Distefano, M. D., and Taton, T. A. (2012) Covalent protein-oligonucleotide conjugates by copper-free click reaction. *Bioorg. Med. Chem. 20*, 4532−4539.
(44) Soundrarajan, N., Sokalingam, S., Raghunathan, G., Budisa, N., Paik, H. J., Yoo, T. H., and Lee, S. G. (2012) Conjugation of proteins by installing BIO-orthogonally reactive groups at their N-termini. *PLoS One 7*, e46741.
(45) Begum, A. A., Radhakrishnan, R., and Nazeer, K. P. (2011) Study of structure-property relationship on sulfuric acid crosslinked chitosan membranes. *Malaysian Polymer Journal 6*, 27−38.
(46) Kumirska, J., Czerwicka, M., Kaczynski, Z., Bychowska, A., Brzozowski, K., Thoming, J., and Stepnowski, P. (2010) Application of spectroscopic methods for structural analysis of chitin and chitosan. *Mar. Drugs 8*, 1567−1636.
(47) Zhang, Z., and Cui, H. (2012) Biodegradability and biocompatibility study of poly(chitosan-g-lactic acid) scaffolds. *Molecules 17*, 3243−3258.
(48) Liao, S., Lin, M., and Hung, C. (2004) A kinetic study of thermal degradations of chitosan/polycaprolactam blends. *Macromol. Res. 12*, 466−473.
(49) Welzel, P. B. (2002) Investigation of adsorption-induced structural changes of proteins at solid/liquid interfaces by differential scanning calorimetry. *Thermochim. Acta 382*, 175−188.
(50) Heron, P. M., Sutton, B. M., Curinga, G. M., Smith, G. M., and Snow, D. M. (2007) Localized gene expression of axon guidance molecules in neuronal co-cultures. *J. Neurosci. Methods 159*, 203−214.
(51) Bernfield, M., Kokenyesi, R., Kato, M., Hinkes, M. T., Spring, J., Gallo, R. L., and Lose, E. J. (1992) Biology of the syndecans: a family of transmembrane heparan sulfate proteoglycans. *Annu. Rev. Cell Biol. 8*, 365−393.
(52) Rutishauser, U., Acheson, A., Hall, A. K., Mann, D. M., and Sunshine, J. (1988) The neural cell adhesion molecule (NCAM) as a regulator of cell-cell interactions. *Science 240*, 53−57.

(53) Nimni, M. E. (1997) Polypeptide growth factors: targeted delivery systems. *Biomaterials 18*, 1201−1225.
(54) Uebersax, L., Merkle, H. P., and Meinel, L. (2009) Biopolymer-based growth factor delivery for tissue repair: from natural concepts to engineered systems. *Tiss. Eng. Part B Rev. 15*, 263−289.
(55) Steffensky, M., Steinbach, K., Schwarz, U., and Schlosshauer, B. (2006) Differential impact of semaphorin 3E and 3A on CNS axons. *Int. J. Dev. Neurosci. 24*, 65−72.
(56) Dontchev, V. D., and Letourneau, P. C. (2002) Nerve growth factor and semaphorin 3A signaling pathways interact in regulating sensory neuronal growth cone motility. *J. Neurosci. 22*, 6659−6669.
(57) Masters, K. S. (2011) Covalent growth factor immobilization strategies for tissue repair and regeneration. *Macromol. Biosci. 11*, 1149−1163.
(58) Ito, Y. (2008) Covalently immobilized biosignal molecule materials for tissue engineering. *Soft Matter 4*, 46−56.
(59) Zhong, X., and Rescorla, F. J. (2012) Cell surface adhesion molecules and adhesion-initiated signaling: understanding of anoikis resistance mechanisms and therapeutic opportunities. *Cell. Signalling 24*, 393−401.
(60) Markus, A., Patel, T. D., and Snider, W. D. (2002) Neurotrophic factors and axonal growth. *Curr. Opin. Neurobiol. 12*, 523−531.
(61) Madduri, S., Papaloizos, M., and Gander, B. (2009) Synergistic effect of GDNF and NGF on axonal branching and elongation in vitro. *Neurosci. Res. 65*, 88−97.
(62) Klimaschewski, L., Nindl, W., Feurle, J., Kavakebi, P., and Kostron, H. (2004) Basic fibroblast growth factor isoforms promote axonal elongation and branching of adult sensory neurons in vitro. *Neuroscience 126*, 347−353.
(63) Gallo, G., and Letourneau, P. C. (1998) Localized sources of neurotrophins initiate axon collateral sprouting. *J. Neurosci. 18*, 5403−5414.
(64) Atwal, J. K., Massie, B., Miller, F. D., and Kaplan, D. R. (2000) The TrkB-Shc site signals neuronal survival and local axon growth via MEK and P13-kinase. *Neuron 27*, 265−277.
(65) Aoki, K., Nakamura, T., and Matsuda, M. (2004) Spatio-temporal regulation of Rac1 and Cdc42 activity during nerve growth factor-induced neurite outgrowth in PC12 cells. *J. Biol. Chem. 279*, 713−719.
(66) MacInnis, B. L., and Campenot, R. B. (2002) Retrograde support of neuronal survival without retrograde transport of nerve growth factor. *Science 295*, 1536−1539.
(67) MacInnis, B. L., Senger, D. L., and Campenot, R. B. (2003) Spatial requirements for TrkA kinase activity in the support of neuronal survival and axon growth in rat sympathetic neurons. *Neuropharmacology 45*, 995−1010.
(68) Liu, B. P., and Strittmatter, S. M. (2001) Semaphorin-mediated axonal guidance via Rho-related G proteins. *Curr. Opin. Cell Biol. 13*, 619−626.
(69) Castellani, V., and Rougon, G. (2002) Control of semaphorin signaling. *Curr. Opin. Neurobiol. 12*, 532−541.
(70) Brown, J. A., and Bridgman, P. C. (2009) Disruption of the cytoskeleton during Semaphorin 3A induced growth cone collapse correlates with differences in actin organization and associated binding proteins. *Dev. Neurobiol. 69*, 633−646.